JOURNAL OF SOLID STATE CHEMISTRY **140,** 431–434 (1998)
ARTICLE NO. SC987864

BRIEF COMMUNICATION

Effect of Ge^{4+} Ion on Electrical Properties of $(La_{0.1}Ca_{0.9})(Mn_{1-x}Ge_x)O_3$

Hideki Taguchi,[1] Masanori Sonoda, and Mahiko Nagao

Research Laboratory for Surface Science, Faculty of Science, Okayama University, Okayama 700-8530, Japan

Received May 16, 1997; in revised form January 13, 1998; accepted April 21, 1998

Orthorhombic perovskite-type $(La_{0.1}Ca_{0.9})(Mn_{1-x}Ge_x)O_3$ was synthesized in the range ($0.00 \le x \le 0.10$). Since the ionic radius of the Ge^{4+} ion is equal to that of the Mn^{4+} ion, the (Mn, Ge)–O(1, 2) distances and the angles for (Mn, Ge)–O(1, 2)–(Mn, Ge) are independent of the composition (x). From the measurement of the electrical resistivity (ρ), all manganates exhibit a metal–insulator transition. With increasing x, the metal–insulator transition temperature (T_t) increases and $d\rho/dT$ decreases. The cation–anion–cation overlap integrals are weakened by the Ge^{4+} ion. © 1998 Academic Press

Orthorhombic perovskite-type $(Ln_{1-x}Ca_x)MnO_3$ (Ln = La, Nd, Gd etc.) exhibits a metal–insulator transition without any crystallographic change (1–4). From the magnetic measurement of these manganates, the spin state of the Mn^{3+} ion changes partly from low to high at the metal–insulator transition temperature (T_t) (1–3). T_t is strongly affected by the composition (x) and the ionic radius of the rare–earth ion (5).

Taguchi *et al*. investigated the role of a tetravalent ion in the metal–insulator transition in $(La_{0.1}Ca_{0.9})(Mn_{1-x}Ti_x)O_3$ (6). With increasing x, the average (Mn, Ti)–O distances increase linearly and the average angles for (Mn, Ti)–O–(Mn, Ti) decrease slightly. The manganates exhibit the metal–insulator transition in the range $0.0 \le x \le 0.3$. From these results, it is obvious that the difference in the ionic radii between the Ti^{4+} and the Mn^{4+} ions makes the cation–anion–cation overlap integrals weaken.

The Ge^{4+} ion has the closed shell of the $3d^{10}$ electrons, and the ionic radius of the Ge^{4+} ion is equal to that of the Mn^{4+} ion (7). Therefore, it is expected that the (Mn, Ge)–O distance will be independent of x. The total number of the $3d$ electrons that participate in the electrical conductivity will increase linearly with increasing x. In the present study, we tried to synthesize $(La_{0.1}Ca_{0.9})(Mn_{1-x}Ge_x)O_3$ samples. These samples are expressed as $(La^{3+}_{0.1}Ca^{2+}_{0.9})[Mn^{3+}_{0.1}(Mn^{4+}_{0.9-x}Ge^{4+}_x)]O_3$. From the relationship between the crystal structure and the electrical properties, we will make a comparison between $(La_{0.1}Ca_{0.9})(Mn_{1-x}Ge_x)O_3$ and $(La_{0.1}Ca_{0.9})(Mn_{1-x}Ti_x)O_3$.

Dried La_2O_3, $CaCO_3$, MnO_2, and GeO_2 powders were weighted in the appropriate proportions and milled for a few hours with acetone. After the mixed powders were dried at 373 K, they were calcined at 1173 K for 12 h in air and then fired at 1573 K for 24 h under a flow of pure oxygen gas. For the measurement of the electrical resistivity, the powders were pressed into a pellet form under a pressure of 50 MPa, and the pellet was sintered at 1573 K for 12 h under a flow of pure oxygen gas. The samples were then annealed at 973 K for 24 h under a flow of pure oxygen gas.

The phases of the samples were identified by X-ray powder diffraction (XRD) with monochromatic Cu$K\alpha$ radiation. The structure refinement was carried out by the Rietveld analysis of the XRD data with the "RIETAN" program written by Izumi (8). The XRD data were collected by step scanning over an angular range of $20 \le 2\theta \le 100^\circ$ in increments of 0.02° (2θ) with monochromatic Cu$K\alpha$ radiation. The electrical resistivity (ρ) of the samples was measured by a standard four-electrode technique in the temperature range 25–973 K. The type of semiconductor, n or p, was identified from the measurement of the thermoelectric effect. The magnetic susceptibility (χ) was measured with a magnetic torsion balance in the temperature range 300–673 K.

In the range $0.00 \le x \le 0.10$, the XRD patterns of $(La_{0.1}Ca_{0.9})(Mn_{1-x}Ge_x)O_3$ were completely indexed as the orthorhombic perovskite-type structure. But, the XRD patterns of the samples ($x \ge 0.15$) gave both the orthorhombic perovskite-type phases and the unknown phases. The structure refinement of $(La_{0.1}Ca_{0.9})(Mn_{1-x}Ge_x)O_3$ was carried out by the Rietveld analysis. The space group of an orthorhombic $GdFeO_3$-type structure is *Pnma* (9). Isotropic thermal parameters (B) for La, Ca, Mn, Ge, O(1), and O(2) ions

[1] To whom all correspondence should be addressed.

0022-4596/98 $25.00

TABLE 1
Refined Structure Parameters for $(La_{0.1}Ca_{0.9})(Mn_{1-x}Ge_x)O_3$

Atom	Position	x	y	z	B
$x = 0.00$, $a = 0.53072(2)$ nm, $b = 0.74943(2)$ nm, $c = 0.53007(2)$ nm $R_{WP} = 12.36\%$, $R_P = 8.65\%$, $R_I = 2.76\%$, $R_F = 2.93\%$					
La, Ca	4(c)	0.027(1)	0.25	− 0.005(2)	0.0027(8)
Mn	4(b)	0	0	0.5	0.0027(8)
O(1)	4(c)	0.491(3)	0.25	0.068(6)	0.0027(8)
O(2)	8(d)	0.286(4)	0.031(3)	− 0.284(4)	0.0027(8)
$x = 0.05$, $a = 0.53074(2)$ nm, $b = 0.74951(2)$ nm, $c = 0.53021(2)$ nm $R_{WP} = 11.89\%$, $R_P = 7.87\%$, $R_I = 3.01\%$, $R_F = 3.73\%$					
La, Ca	4(c)	0.027(1)	0.25	− 0.004(3)	0.0026(8)
Mn, Ge	4(b)	0	0	0.5	0.0026(8)
O(1)	4(c)	0.488(3)	0.25	0.070(7)	0.0026(8)
O(2)	8(d)	0.286(4)	0.030(3)	− 0.282(4)	0.0026(8)
$x = 0.10$, $a = 0.53067(2)$ nm, $b = 0.74927(3)$ nm, $c = 0.53011(2)$ nm $R_{WP} = 11.67\%$, $R_P = 8.02\%$, $R_I = 3.22\%$, $R_F = 3.37\%$					
La, Ca	4(c)	0.026(1)	0.25	− 0.004(3)	0.0009(7)
Mn, Ge	4(b)	0	0	0.5	0.0009(7)
O(1)	4(c)	0.491(3)	0.25	0.070(7)	0.0009(7)
O(2)	8(d)	0.281(4)	0.030(3)	− 0.285(4)	0.0009(7)

were refined assuming that they had the same values. Refined structure parameters are summarized in Table 1. The cell constants (a, b, and c axes) are independent of x. R_{WP}, R_P, R_I, and R_F are the R factors of the weighted pattern, the pattern, the integrated intensity, and the structure factor, respectively.

The ionic radii of the Mn^{4+}, Ge^{4+}, and Ti^{4+} ions with a coordination number (CN) of 6 are 0.054, 0.054, and 0.0605 nm, respectively (7). Therefore, it is considered that the cell constants of $(La_{0.1}Ca_{0.9})(Mn_{1-x}Ge_x)O_3$ are independent of x, while the cell constants of $(La_{0.1}Ca_{0.9})(Mn_{1-x}Ti_x)O_3$ increase linearly with increasing x (6). In the orthorhombic $GdFeO_3$-type structure, the La and Ca ions coordinate with twelve anions; four O(1) and eight O(2) ions. The Mn and Ge ions coordinate with six anions; two O(1) and four O(2) ions. There are two kinds of the cation–anion–cation overlap integrals (Δ^{π}_{cac} and Δ^{σ}_{cac}); Δ^{π}_{cac} is the overlap integral between the cation $d\varepsilon$* and oxygen p_π orbitals, and Δ^{σ}_{cac} is the overlap integral between the cation $d\gamma$* and oxygen p_σ orbitals (10). The (Mn, Ge)–O(1, 2) distances calculated from the refined structural parameters are shown in Table 2. The (Mn, Ge)–O distances are independent of x. The angles for O–(Mn, Ge)–O and (Mn, Ge)–O–(Mn, Ge) are calculated from the refined structural parameters. The angles for O(1)–(Mn, Ge)–O(1), O(1)–(Mn, Ge)–O(2), and O(2)–(Mn, Ge)–O(2) is 180, 90, and 90 or 180°, respectively. The angles for (Mn, Ge)–O(1, 2)–(Mn, Ge) are shown in Table 3. They are less than 180° and independent of x. Since the Ge^{4+} has the closed shell of $3d^{10}$ electrons, it is considered that the cation–anion–cation overlap integrals (Δ^{π}_{cac} and Δ^{σ}_{cac}) are weakened by increasing the Ge^{4+} ion.

TABLE 2
(Mn, Ge)–O Distances (nm) of $(La_{0.1}Ca_{0.9})(Mn_{1-x}Ge_x)O_3$

x	(Mn, Ge)–O(1)	(Mn, Ge)–O(2) × 2	(Mn, Ge)–O(2) × 2
0.00	0.191(1)	0.190(3)	0.192(3)
0.05	0.191(1)	0.189(3)	0.192(3)
0.10	0.191(1)	0.188(3)	0.192(3)

From the measurements of the electrical resistivity (ρ) and the thermoelectric effect of $(La_{0.1}Ca_{0.9})(Mn_{1-x}Ge_x)O_3$, all manganates are n-type semiconductors at low temperature. The energy gap (E_g) calculated from the linear portion of the log ρ–$1000/T$ curves is ≈ 0.08 eV for $x = 0.00$, ≈ 0.11 eV for $x = 0.05$, and ≈ 0.14 eV for $x = 0.10$, respectively. Figure 1 shows the relationship between ρ and temperature (T). ρ has a positive temperature coefficient at high temperature and increases linearly with increasing temperature. These results indicate that $(La_{0.1}Ca_{0.9})(Mn_{1-x}Ge_x)O_3$ exhibits the metal–insulator transition as well as $(La_{0.1}Ca_{0.9})(Mn_{1-x}Ti_x)O_3$ ($0 \le x \le 0.3$). In $(La_{0.1}Ca_{0.9})(Mn_{1-x}Ge_x)O_3$, T_t is ≈ 305 K ($x = 0.00$), ≈ 395 K ($x = 0.05$), and ≈ 625 K ($x = 0.10$). $d\rho/dT$ decreases with increasing x; $\approx 3.4 \times 10^{-6}\,\Omega\cdot$cm/K ($x = 0.00$), $\approx 2.9 \times 10^{-6}\,\Omega\cdot$cm/K ($x = 0.05$), and $\approx 1.9 \times 10^{-6}\,\Omega\cdot$cm/K ($x = 1.00$).

The total number of $3d$ electrons (n_{total}) per formula unit of $(La_{0.1}Ca_{0.9})(Mn_{1-x}Ge_x)O_3$ is $(3.1 + 7x)$. The relationship among T_t, $d\rho/dT$, and n_{total} in $(La_{0.1}Ca_{0.9})(Mn_{1-x}A_x)$ O_3 (A = Ge, Ti) is shown in Fig. 2. With increasing n_{total}, T_t varies parabolically and $d\rho/dT$ decreases. Figure 3 shows the $1/\chi$–T curve of $(La_{0.1}Ca_{0.9})(Mn_{0.95}Ge_{0.05})O_3$ ($x = 0.05$). We can observe the deflection at 400–440 K, and this deflection corresponds nearly to T_t. The effective magnetic moment (μ_{eff}) calculated from the $1/\chi$–T curve is $\approx 3.76 \pm 0.01\,\mu_B$ in the range 300–400 K, and $\approx 3.81 \pm 0.01\,\mu_B$ in the range 430–673 K, respectively. These results indicate that the spin state of the Mn^{3+} ion changes partly from low to high. Above $n_{total} = 3.0$, the metal–insulator transition of $(La_{0.1}Ca_{0.9})$ $(Mn_{1-x}A_x)O_3$

TABLE 3
(Mn, Ge)–O–(Mn, Ge) Angles (deg) for $(La_{0.1}Ca_{0.9})(Mn_{1-x}Ge_x)O_3$

x	(Mn, Ge)–O–(1)–(Mn, Ge)	(Mn, Ge)–O(2)–(Mn, Ge)
0.00	157.9(20)	158.8(10)
0.05	157.2(21)	159.5(11)
0.10	157.5(21)	159.7(11)

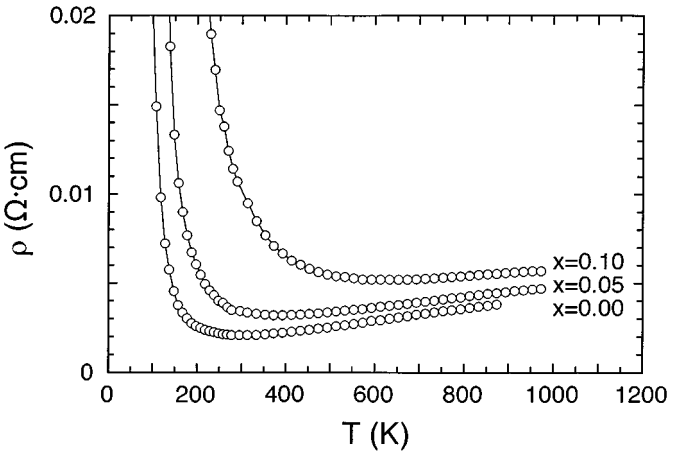

FIG. 1. Electrical resistivity (ρ) vs temperature (T) for the system $(La_{0.1}Ca_{0.9})(Mn_{1-x}Ge_x)O_3$.

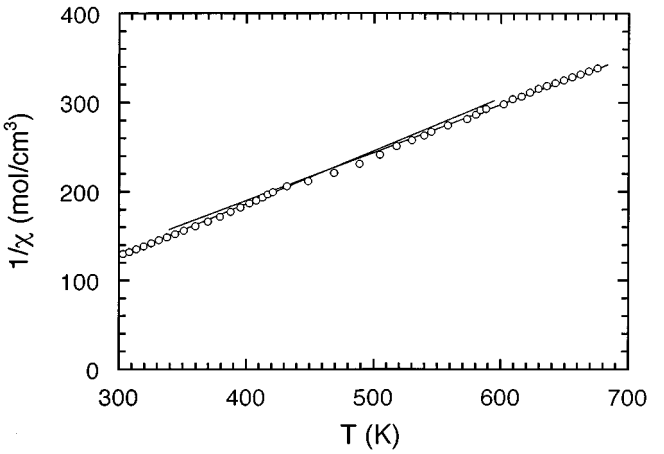

FIG. 3. Inverse magnetic susceptibility ($1/\chi$) vs temperature (T) for $(La_{0.1}Ca_{0.9})(Mn_{0.95}Ge_{0.05})O_3$ ($x = 0.05$).

(A = Ge, Ti) is explained by the band model proposed by Goodenough (10, 11). At low temperature, the 3d electrons coexist in the localized π^*–α and π^*–β orbitals. At high temperature, the spin state of the Mn^{3+} ion changes partly from low to high. Since the 3d electrons coexist in the localized π^*–α and the collective σ^*–α orbitals, $(La_{0.1}Ca_{0.9})(Mn_{1-x}A_x)O_3$ (A = Ge, Ti) exhibits the metal–insulator transition. T_t has a minimum value at $n_{total} = 3.1$. The variation of T_t in the range $3.0 \le n_{total} \le 3.1$ depends on the cation–anion–cation overlap integrals (Δ^{π}_{cac} and Δ^{σ}_{cac}) in $(La_{0.1}Ca_{0.9})(Mn_{1-x}Ti_x)O_3$ (6). In $(La_{0.1}Ca_{0.9})(Mn_{1-x}Ge_x)O_3$, the Ge^{4+} weakens the cation–anion–cation overlap integrals (Δ^{π}_{cac} and Δ^{σ}_{cac}), and T_t increases above $n_{total} \ge 3.1$. The increase in the number of the 3d electrons in the collective σ^* orbital makes $d\rho/dT$ decrease.

It is concluded that Rietveld analysis of $(La_{0.1}Ca_{0.9})(Mn_{1-x}Ge_x)O_3$ ($0.00 \le x \le 0.10$) indicates that the (Mn, Ge)–O(1, 2) distances and the angles for (Mn, Ge)–O(1, 2)–(Mn, Ge) are independent of x. $(La_{0.1}Ca_{0.9})(Mn_{1-x}Ge_x)O_3$ exhibits the metal–insulator transition. The cation–anion–cation overlap integrals (Δ^{π}_{cac} and Δ^{σ}_{cac}) are weakened by the Ge^{4+} ion, and T_t increases with increasing x. The decrease of $d\rho/dT$ is caused by the increase of the 3d electrons in the collective σ^* orbtal.

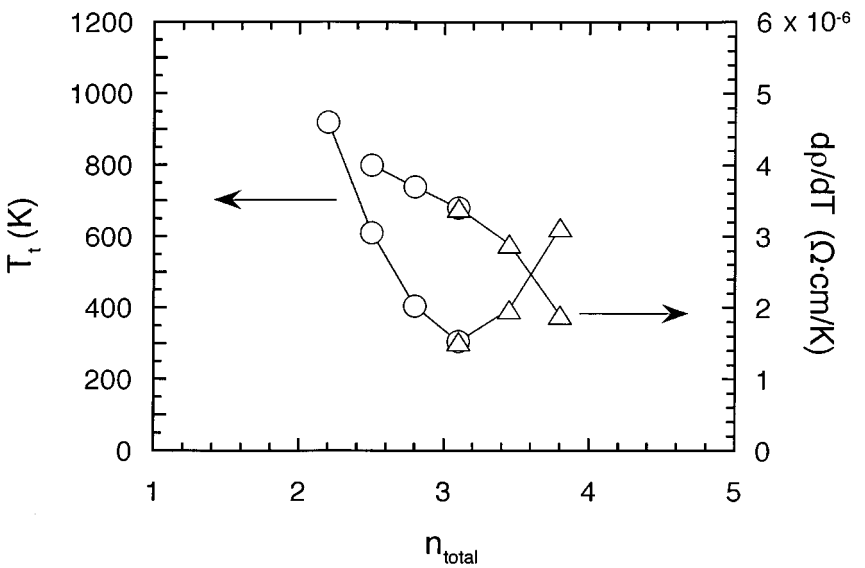

FIG. 2. Relationship among the metal–insulator transition temperature (T_t), $d\rho/dT$, and the total number of 3d electrons (n_{total}) in $(La_{0.1}Ca_{0.9})(Mn_{1-x}A_x)O_3$ (A = Ge, Ti). (△) $(La_{0.1}Ca_{0.9})(Mn_{1-x}Ge_x)O_3$; (○) $(La_{0.1}Ca_{0.9})(Mn_{1-x}Ti_x)O_3$ (6).

ACKNOWLEDGMENT

The authors express their thanks to Dr. H. Kido, Osaka Municipal Technical Institute, for the magnetic measurements.

REFERENCES

1. H. Taguchi and M. Shimada, *J. Solid State Chem.* **63,** 290 (1986).
2. H. Taguchi, M. Nagao, and M. Shimada, *J. Solid State Chem.* **76,** 284 (1988).
3. H. Taguchi, M. Nagao, and M. Shimada, *J. Solid State Chem.* **82,** 8 (1989).
4. T. Kobayahi, H. Takizawa, T. Endo, T. Sato, M. Shimada, H. Taguchi, and M. Nagao, *J. Solid State Chem.* **92,** 116 (1991).
5. H. Taguchi, M. Nagao, and M. Shimada. *J. Solid State Chem.* **97,** 476 (1992).
6. H. Taguchi, M. Sonoda, M. Nagao, and H. Kido, *J. Solid State Chem.* **126,** 235 (1996).
7. R. D. Shannon and C. T. Prewitt, *Acta Crystallogr., Sect. B* **25,** 925 (1969).
8. F. Izumi, "The Rietveld Method," p. 236. Oxford Univ. Press, Oxford, 1993.
9. K. R. Poeppelmeier, M. E. Leonowicz, J. C. Scanlon, and W. B. Yelon, *J. Solid State Chem.* **45,** 71 (1982).
10. J. B. Goodenough, *Czech. J. Phys. B* **17,** 304 (1967).
11. J. B. Goodenough, *J. Appl. Phys.* **37,** 1415 (1966).